# State-of-the-art $\gamma$-ray assay of $^{86}$Y for medical imaging

A. C. Gula,[1,2] E. A. McCutchan,[2] C. J. Lister,[3] J. P. Greene,[4] S. Zhu,[2,4] P. A. Ellison,[5] R. J. Nickles,[5] M. P. Carpenter,[4] Suzanne V. Smith,[6] and A. A. Sonzogni[2]

[1]*Department of Physics Computer Science, Houghton College, Houghton, New York 14744, USA*
[2]*National Nuclear Data Center, Brookhaven National Laboratory, Upton, New York 11973, USA*
[3]*Department of Physics and Applied Physics, University of Massachusetts Lowell, Lowell, Massachusetts 01854, USA*
[4]*Physics Division, Argonne National Laboratory, Argonne, Illinois 60439, USA*
[5]*Department of Medical Physics, University of Wisconsin - Madison, Madison, Wisconsin 53706, USA*
[6]*Regmentsgatan 12, Malmo 21142, Sweden*

(Received 3 July 2019; revised 26 June 2020; accepted 31 July 2020; published 11 September 2020)

An emerging direction in nuclear medicine is the coupling of a therapeutic isotope with an imaging isotope to form a so-called theranostic pair, which allows one to quantitatively track and image the delivery of the therapeutic isotope. $^{90}$Y is used in several therapy applications and a convenient candidate imaging partner is the positron emitter $^{86}$Y. A 27.6 MBq source of $^{86}$Y was produced at the University of Wisconsin and assayed with the Gammasphere array at Argonne National Laboratory. Over 200 $\gamma$-ray transitions were identified, more than double that which was previously known. The positron emission probability inferred from the present level scheme leads to 27.9(12)%, an important ($\approx$14%) reduction with respect to the previously recommended value.

DOI: 10.1103/PhysRevC.102.034316

## I. INTRODUCTION

$^{90}$Y is an excellent isotope for medical therapy. The decay [1] is a 99.99% ground state-to-ground state $\beta^-$ decay with a $Q$ value of 2.28 MeV, so produces electrons with a mean energy of approximately 900 keV which can cause severe, but local, tissue damage. It has a 64 hour half-life, which is good for production and delivery, but can yield high specific activity and it decays away quickly after use. It also has good chemical properties which allow the radioisotope to be packaged or attached to molecules and delivered to specific sites.

Simultaneous, quantitative PET (positron emission tomography) studies with $^{90}$Y are sometimes possible [2], but difficult due to the tiny branching ratio for positron emission via internal pair creation in the $0_2^+ \rightarrow 0_1^+$ transition in the $^{90}$Zr daughter. Only $31.86(47) \times 10^{-6}$ positrons are emitted per $^{90}$Y decay [3] which limits $^{90}$Y PET to few specific clinical applications. For theranostic applications, a potential partner is the isotope $^{86}$Y which has exactly the same chemistry and the ground state $T_{1/2} = 14.74$ h decay has a strong positron emission branch so can used for reliable PET imaging and dose estimates. The $^{86}$Y - $^{90}$Y pair has been investigated for labeling antibodies and peptides in a number of studies [4–8]. For clinical applications, the decay properties of $^{86}$Y need improvement in order to allow more reliable estimates of yttrium delivery to specific sites. Precisely quantifying the $^{86}$Y decay data is the main goal of this research, although interesting new structural information may also emerge.

The full $\epsilon + \beta^+$ scheme of $^{86}$Y was last studied more than 40 years ago before big arrays of gamma detectors had evolved. The first measurement of $^{86}$Y decay identified around 80 transitions [9]. The evaluated data [10] is based mainly on a later experiment by Ramayya *et al.* [11], where approximately 100 $\gamma$-ray transitions were identified and placed. Several of the weaker transitions observed in Ref. [9], were not confirmed by Ref. [11]. Select angular correlations were studied in Ref. [12]. In the decades which followed these decay experiments on $^{86}$Y, the technological capabilities of $\gamma$-ray spectroscopy have advanced tremendously. Given the potential medical application interest in $^{86}$Y, we performed a new gamma-ray spectroscopy experiment using the Gammasphere array at Argonne National Laboratory to provide a rigorous and more complete decay scheme for $^{86}$Y. The $\gamma$-ray emissions were precisely quantified down to an intensity level of $<$0.0001% of the strongest $\gamma$-ray transition emitted in the decay. With this new decay scheme, we are able to deduce the positron emission intensity, the quantity relevant to use of $^{86}$Y as a PET imaging agent.

## II. EXPERIMENT

A source of $^{86}$Y was produced via the $^{86}$Sr$(p, n)$ reaction by irradiating a $^{86}$Sr target with 16 MeV protons from the University of Wisconsin Medical Physics cyclotron. An isotopically enriched $^{86}SrCO_3$ (96.4%, ISOFLEX) was pressed into a niobium pocket (0.41 mm deep, 1.2 cm diameter) and covered with a 51 $\mu$m niobium foil. The target was placed in a solid target support that seals the rear surface against a jet of water for heat dissipation. Irradiations were performed on a 16 MeV proton GE PETtrace cyclotron with a current of 4 $\mu$A. The production yields are $0.100 \pm 0.015$ GBq/$\mu$Ah at end of bombardment (EoB) including the contribution from total decay of $^{86m}$Y ($T_{1/2} = 48$ min). The target was irradiated for 1 h.

 

After irradiation, the target was dismounted, placed in a beaker and the $SrCO_3$ was dissolved in 9 M HCl. This target solution was then transferred to the reservoir syringe connected to a peristaltic pump-driven automated module [13], from which the solution was directed to a 0.5 cm diameter column filled with 100 mg of DGA resin ($N, N, N', N'$-tetrakis-2-ethylhexyldiglycolamide, Eichrom) at a flow rate of 1.1 mL/min, which trapped the $^{86}$Y. A wash of 9 M HCl solution was employed to wash away impurities. The loading and washing solutions were combined and the $^{86}SrCO_3$ was recycled following published methods [14,15]. The elution was carried out by pumping 200 $\mu$L fractions of 1 M HCl through the loaded resin and the three most concentrated eluates were combined, evaporated to dryness and the residue was redissolved in 100 $\mu$L of 0.1 M HCl. The radionuclidic purity of $^{86}$Y 12 h post-EoB was 98.3%, the recycling yield of $^{86}SrCO_3$ was $90 \pm 3\%$ and the $^{86}$Y separation efficiency was $94 \pm 5\%$.

Upon arrival to Argonne National Laboratory 24 h later, the estimated source activity was 27.6 MBq. The original source was subdivided into 5%, 15%, and 80% portions so that the source decay could be recorded over several days at a rate acceptable for the digital Gammasphere data acquisition system. The 15% and 80% subdivisions were introduced when the total singles rate fell below $10^5$ events per second. The total counting period was 6 d. During the Gammasphere assay, both single $\gamma$-ray and double $\gamma$-ray coincidence triggers were recorded. In the present work, 32 detectors were selected for the data analysis. The other detectors were not considered due to significant neutron damage.

In the present experiment $6.3 \times 10^9$ single $\gamma$-ray and $2.9 \times 10^9$ double $\gamma$-ray coincidence triggered events were recorded and analyzed. Because of the large data set, a $\gamma$-$\gamma$-$\gamma$ coincidence cube could be constructed and proved essential for discerning the placement of the many degenerate energy transitions in $^{86}$Y. The singles spectrum following the decay of $^{86}$Y is given in Fig. 1(a) illustrating the high density of observed transitions. A sample spectrum, gated on the 1076-keV, $2_1^+ \rightarrow 0_1^+$ transition in the daughter $^{86}$Sr is shown in Fig. 1(b), highlighting the quality of the $\gamma$-$\gamma$ data. Comparing our spectra to the sample $\gamma$-$\gamma$ coincidence spectra in Ref. [11], we estimate the current experiment resulted in an improvement of over 3 orders of magnitude in statistics.

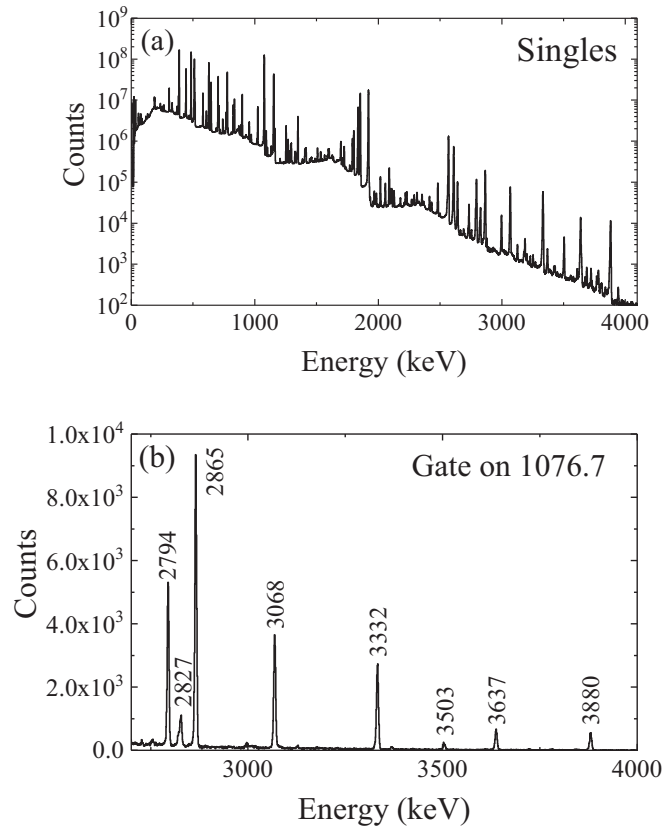


FIG. 1. (a) Singles spectrum from the decay of $^{86}$Y. (b) Background subtracted doubles spectrum gated on the 1076.7-keV, $2_1^+ \rightarrow 0_1^+$ transition in $^{86}$Sr, highlighting the high energy region. Strong transitions are labeled by their energy in keV.

## III. DATA ANALYSIS

Data were sorted using the GSSort [16] package to construct $\gamma$-ray singles spectra, $\gamma$-$\gamma$ coincidence matrices, and $\gamma$-$\gamma$-$\gamma$ coincidence cubes. A 30 ns timing coincidence window software requirement was placed for the construction of the $\gamma$-$\gamma$ coincidence matrix as well as the $\gamma$-$\gamma$-$\gamma$ coincidence cube. The data analysis was performed using a modified version of the RADWARE package GF3 [17].

The energy calibration was performed using standard sources of $^{182}$Ta [18], $^{152}$Eu [19], and $^{56}$Co [21]. A systematic error of 0.1% for all energies, is included in the values reported here, added in quadrature to the statistical uncertainty. The efficiency calibration of Gammasphere followed the procedure described in Ref. [22] using the very well-known transitions in the decay of $^{182}$Ta [18], $^{152}$Eu [19], $^{88}$Y [20], and $^{56}$Co [21]. A minimum systematic uncertainty of 2% was included in the intensity measurements, again added in quadrature to the statistical uncertainties.

Most of the $\gamma$-ray intensities were determined by "gating from below" on transitions depopulating a level and measuring the area of a transition feeding into the level. This area was corrected for the efficiency of the array at the $\gamma$ ray energy observed as well as the efficiency for the energy of the transition used in the gate from below. Corrections for the branching of the $\gamma$-ray transition were also applied. Due to the symmetry of Gammasphere, angular correlation corrections were found to be negligible. Even with the down select of a subset of Gammasphere detectors, the coverage of detector angle pairs between 20° and 159° remained similar to the full array.

The procedure to obtain the transition intensity follows that as described in Ref. [22]. When possible, multiple gates from below were taken and the resulting intensities compared to check for possible underlying doublets. The intensities of $\gamma$-ray transitions were most commonly a weighted mean of the gates from below. In addition, there were several transitions that gating from below proved difficult or impossible. In order to determine the intensities for such transitions, a "gate from above" was taken on a transition populating the level and

measuring the intensity of the transition of interest relative to a well-known transition intensity which was previously determined in a gate from below. All transition intensities were measured relative to the 1076.7-keV $2_1^+ \rightarrow 0_1^+$ transition, taking $I\gamma(1076.7) = 100$.

Angular correlations were investigated by taking advantage of the numerous detector angles available in Gammasphere. The angle pairs where binned into 18 groupings at 20°, 35°, 40°, 52°, 54°, 60°, 66°, 70°, 72°, 74°, 86°, 90°, 93°, 100°, 105°, 125°, 139°, and 159°. The angle bin efficiencies were determined by finding the number of counts in each transition peak in a cascade pair and comparing it to the total number of counts in each transition peak in the singles spectrum where all of the detectors were combined together.

A few contaminants were identified in the source. $^{87}$Y, with a 79.8 h half-life, was weakly observed in the present experiment. The decay of $^{87}$Y populates 100% a 873-keV level in $^{87}$Sr, which decays by a 484-keV transition into a 388-keV isomeric level ($T_{1/2} = 2.8$ h), which subsequently decays via a single 388-keV transition [23]. From the singles spectrum, it was determined that for every thousand decays of $^{86}$Y, there were only two decays of a $^{87}$Y nucleus. As the decay results in only these two well-characterized transitions, the $^{87}$Y did not complicate the present analysis.

A contaminant of $^{88}$Y, ($T_{1/2} = 106.6$ d), was also observed very weakly within the $\gamma$-$\gamma$ coincidence matrix. In singles, we observed three decays for every $10^4$ decays of $^{86}$Y. As this contaminant is very weak and only produces six, well-characterized transitions [20], among which the 897- and 1835-keV transitions are predominant, it also could be easily accounted for in the present experiment.

$^{86}$Y has a high-spin isomeric state, $J^\pi = 8^+$, $E = 218$ keV [10] which in principle could be populated in the $(p, n)$ reaction. This state has a half-life of 48 min and decays mainly (99.31%) via internal electromagnetic (IT) decay. The 0.69% $\epsilon + \beta^+$ branch directly populates the yrast $8^+$, 2956-keV level of $^{86}$Sr. If this decay was present in the current experiment, a 98-keV $8_1^+ \rightarrow 6_1^+$ transition would be observed in coincidence with the lower yrast band transitions. No evidence for a 98-keV transition was observed in coincidence spectra, thus if produced, the 24-h cooling period and small $\epsilon + \beta^+$ branch result in a presence of $^{86m}$Y which is below the level of sensitivity of the current experiment.

## IV. EXPERIMENTAL RESULTS

Table I lists the energies and intensities of the $\gamma$-rays observed in this analysis and were assigned to the decay of $^{86}$Y. The previous decay scheme of $^{86}$Y consisted of 31 levels and 104 placed $\gamma$-ray transitions [10]. In the present work, we more than double the number of observed transitions and identify 20 additional excited levels. We confirm all levels previously proposed in $\beta$ decay [11] with one exception. The 4339-keV level proposed in Ref. [11] as a tentative state with only one decay transition was eliminated based on non observation of the 1154-keV decay transition into the 2997-keV level. No evidence for this transition was found in cleanest gates on the strongest decay transitions from the 2997-keV level nor in any other gate in the present work.

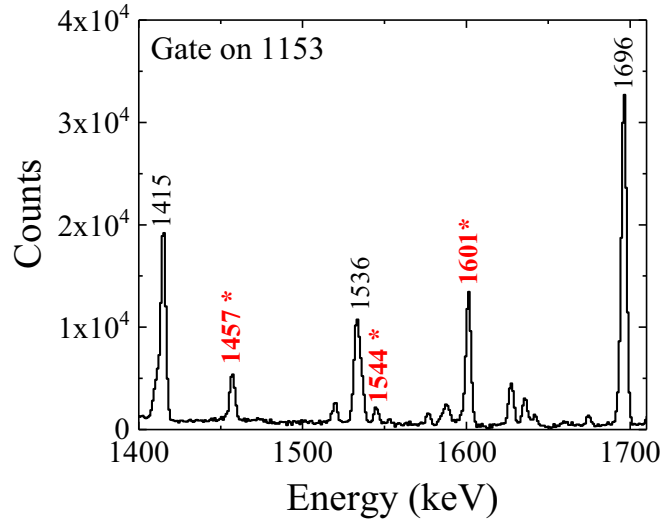


FIG. 2. Spectrum obtained by gating on the 1153-keV, $4_1^+ \rightarrow 2_1^+$ transition. Transitions identified as directly populating the $4_1^+$ level are labeled by their energy in keV. Transitions not included in the evaluated data [10] but identified and placed in the present work are given in red and indicated with an asterisk.

Several of the previously unplaced transitions observed in Ref. [9] could now be placed in the level scheme based on our high-statistics $\gamma$-$\gamma$ coincidence analysis. These include the previously reported [9] 118.7(5)-, 1390(2)-,1460(1)-, 1603(2)-, 1661(2)-, 1940(3)-, 2058(2)-, 2314(3)-, 2617(2)-, and 3865(5)-keV transitions which we identify with the transitions observed in present work at 118.96(12), 1385.70(12), 1457.02(10), 1601.05(8) 1663.9(3), 1935.97(8), 2056.84(8), 2312.87(12), 2619.4(3), and 3871.2(4) keV, respectively. These transitions were excluded in the previously evaluated data [10] as they were not confirmed in subsequent studies [11]. Our high statistics work provides excellent support for their placement. As an example, Fig. 2 provides a spectrum gated on the 1153 keV, $4_1^+ \rightarrow 2_1^+$ transition. The strong 1415-, 1536-, and 1696-keV transitions were previously placed as populating the $4_1^+$ level. The present analysis now definitely places the 1457-keV and 1601-keV transitions (previously observed only in Ref. [9]) and identifies a new 1544-keV transition, all populating the $4_1^+$ level.

### A. Discussion of levels

For the decay of the low-lying $2_1^+$, $2_2^+$, $4_1^+$, $3_1^-$, and $2_3^+$ levels, the results of the present measurement are in excellent agreement with the transition intensities determined in Ref. [11] (see Table I). Our high statistics coincidence data has allowed considerable reduction in the uncertainty of the intensity of the weaker transitions, which were previously measured with ~25% uncertainty [11].

The $5_1^-$ 2672-keV level was previously observed to decay via 191- and 443-keV transitions to the $3_1^+$ and $4_1^+$ levels, respectively. In the present work we observe a 1596-keV transition corresponding to the $E3$ decay to the $2_1^+$ level. The 1596-keV transition was identified in all gates on strong transitions feeding the 2672-keV level as well as in a gate on

TABLE I. Levels populated in $^{86}$Sr and their $\gamma$-ray decay. Level energies are determined using a least-squares fit to all measured $\gamma$-ray energies. Spin/parity assignments are from Ref. [10], except where noted. Relative intensities for the depopulating $\gamma$-ray transitions are given by $I_\gamma$. Intensities are normalized to $I_\gamma(1076\gamma) = 100$. The $I_\gamma$'s are also compared with literature values [11] when available. A "W" in the literature intensity column indicates a weak transition.

| $J_i^\pi$ | $E_i$ (keV) | $J_f^\pi$ | $E_f$ (keV) | $E_\gamma$ (keV) | $I_\gamma$ | $\delta$ | $I_\gamma^{lit}$([11]) |
|---|---|---|---|---|---|---|---|
| $2^+$ | 1076.63(5) | $0^+$ | 0.00 | 1076.66(9) | 100(2) | | 100(2) |
| $2^+$ | 1853.90(5) | $2^+$ | 1076.63 | 777.14(8) | 26.2(7) | +0.33(5) | 27.2(7) |
| | | $0^+$ | 0.00 | 1853.82(8) | 20.4(4) | | 20.8(6) |
| $4^+$ | 2229.50(5) | $2^+$ | 1076.63 | 1152.82(8) | 37.0(9) | −0.034(8) | 37.0(11) |
| $3^-$ | 2481.48(5) | $4^+$ | 2229.50 | 251.86(8) | 0.482(12) | | 0.45(2) |
| | | $2^+$ | 1853.90 | 627.50(8) | 39.8(9) | +0.017(6) | 39.5(12) |
| | | $2^+$ | 1076.63 | 1405.01(11) | 0.310(10) | | 0.22(6) |
| | | $0^+$ | 0.00 | 2481.30(10) | 0.179(6) | | 0.14(1) |
| $2^+$ | 2641.15(5) | $2^+$ | 1076.63 | 1564.48(8) | 0.140(15) | | 0.22(6) |
| | | $0^+$ | 0.00 | 2641.15(8) | 0.226(25) | | 0.20(5) |
| $5^-$ | 2672.44(5) | $3^-$ | 2481.48 | 190.81(11) | 1.074(25) | | 1.23(4) |
| | | $4^+$ | 2229.50 | 442.84(8) | 18.7(6) | +0.019(10) | 20.5(6) |
| | | $2^+$ | 1076.63 | 1595.93(12)[b] | 0.322(10) | | |
| $2^+$ | 2787.30(8) | $2^+$ | 1076.63 | 1710.7(2) | 0.181(6) | | 0.21(4) |
| | | $0^+$ | 0.00 | 2787.3(2) | 0.070(7) | | 0.013(7) |
| $6^+$ | 2856.62(8)[aa] | $4^+$ | 2229.50 | 627.23(15)[b] | 0.78(5) | | |
| $3^+$[f] | 2877.90(5) | $4^+$ | 2229.50 | 648.53(8) | 0.424(12) | | *W* |
| | | $2^+$ | 1853.90 | 1023.94(8) | 4.7(3) | +0.42(3) | 4.6(2) |
| | | $2^+$ | 1076.63 | 1801.23(8) | 2.15(6) | +7.2(13) | 2.00(6) |
| $3^-$ | 2996.81(5) | $2^+$ | 2641.15 | 355.67(8) | 0.315(10) | | 0.12(3) |
| | | $3^-$ | 2481.48 | 515.3(1) | 3.78(12) | | 5.93(17) |
| | | $4^+$ | 2229.50 | 767.20(10) | 1.85(6) | | 2.9(13) |
| | | $2^+$ | 1853.90 | [1142.6] | <0.0083 | | 0.12(4) |
| | | $2^+$ | 1076.63 | 1920.12(8) | 26.4(6) | +0.035(4) | 25.2(8) |
| | | $0^+$ | 0.00 | 2997.02(20) | 0.0457(28) | | 0.010(5) |
| $5^-$ | 3055.45(6) | $5^-$ | 2672.44 | 382.76(14) | 3.03(10) | −0.09(6) | 4.40(14) |
| | | $4^+$ | 2229.50 | 825.83(13) | 4.40(12) | −0.01(3) | 4.0(1) |
| $(3, 4^+)$[g] | 3133.50(10)[a] | $2^+$ | 1076.63 | 2056.84(8)[e] | 0.137(4) | | |
| $(3, 4^+)$[g] | 3175.50(10)[a] | $2^+$ | 1076.63 | 2098.84(8)[b] | 0.083(3) | | |
| $3^-$[h] | 3184.75(6) | $5^-$ | 3055.45 | 129.1(2)[b] | 0.0428(12) | | |
| | | $3^-$ | 2996.81 | 187.79(14) | 1.58(5) | | 1.53(5) |
| | | $3^+$ | 2877.90 | 306.76(8) | 4.04(12) | −0.08(3) | 4.2(1) |
| | | $5^-$ | 2672.44 | 512.42(8) | 2.56(8) | | *W* |
| | | $3^-$ | 2481.48 | 703.12(8) | 18.9(5) | +0.54(21) | 18.7(5) |
| | | $4^+$ | 2229.50 | 955.22(9) | 1.42(5) | | 1.26(5) |
| | | $2^+$ | 1076.63 | 2108.22(12) | 0.090(4) | | 0.06(1) |
| $6^-$ | 3290.88(6) | $5^-$ | 3055.45 | 235.23(10) | 0.49(3) | | 0.48(2) |
| | | $6^+$ | 2856.62 | 434.21(8)[b] | 0.147(22) | | |
| | | $2^+$ | 2787.30 | [503] | [d] | | 0.11(4) |
| | | $5^-$ | 2672.44 | 618.45(8) | 0.225(20) | | 0.26(4) |
| $4^-$[f] | 3317.54(6) | $3^-$ | 3184.75 | 132.6(2) | 0.262(10) | | 0.20(1) |
| | | $3^+$ | 2877.90 | 439.59(12) | 1.03(3) | | 0.24(8) |
| | | $5^-$ | 2672.44 | 644.98(9) | 3.14(10) | | 2.65(40) |
| | | $3^-$ | 2481.48 | 835.94(8) | 5.01(15) | +1.0(4) | 5.3(7) |
| | | $4^+$ | 2229.50 | 1088.08(16) | 0.163(6) | | 0.05(1) |
| $4^+$ | 3361.39(6) | $5^-$ | 2672.44 | 688.76(11) | 0.120(4) | | 0.21(4) |
| | | $4^+$ | 2229.50 | 1131.85(15) | 0.171(5) | +0.22(11) | 0.36(3) |
| | | $2^+$ | 1853.90 | 1507.48(8) | 0.438(13) | | 0.43(5) |
| | | $2^+$ | 1076.63 | 2284.61(18)[b] | 0.0279(11) | | |
| | 3389.62(8)[a] | $2^+$ | 1853.90 | 1535.81(15)[b] | 0.0247(8) | | |
| | | $2^+$ | 1076.63 | 2312.87(12)[e] | 0.0493(15) | | |
| $2^+$ | 3430.12(10)[a] | $2^+$ | 1076.63 | 2353.7(2)[b] | 0.0533(15) | | |
| | | $0^+$ | 0.00 | 3429.94(20)[b] | 0.00089(10) | | |

TABLE I. (*Continued.*)

| $J_i^\pi$ | $E_i$ (keV) | $J_f^\pi$ | $E_f$ (keV) | $E_\gamma$ (keV) | $I_\gamma$ | $\delta$ | $I_\gamma^{lit}$([11]) |
|---|---|---|---|---|---|---|---|
| $(3, 4^+)^g$ | 3490.86(10)[a] | $4^+$ | 2229.50 | 1261.09(18)[b] | 0.0555(15) | | |
| | | $2^+$ | 1853.90 | 1636.9(2)[b] | 0.0602(15) | | |
| | | $2^+$ | 1076.63 | 2414.17(14)[b] | 0.041(2) | | |
| $4^{-f}$ | 3499.53(6) | $4^-$ | 3317.54 | 181.77(11)[e] | 0.118(4) | | 0.13(4) |
| | | $5^-$ | 3055.45 | 443.70(25) | 0.977(25) | | 0.78(20) |
| | | $3^-$ | 2481.48 | 1018.05(12) | 0.256(10) | | 0.22(14) |
| | | $4^+$ | 2229.50 | 1270.05(10) | 0.780(20) | −0.05(9) | 0.79(12) |
| $(5)^g$ | 3555.40(6) | $4^-$ | 3317.54 | 237.68(10) | 0.154(5) | | 0.16(3) |
| | | $6^-$ | 3290.88 | 264.29(10) | 0.54(3) | | 0.65(3) |
| | | $6^+$ | 2856.62 | 698.84(8)[b] | 0.575(16) | | |
| | | $5^-$ | 2672.44 | 882.93(8) | 0.497(15) | | 0.3(1) |
| | | $4^+$ | 2229.50 | 1325.93(15)[b] | 0.0115(5) | | |
| $(3^-)$ | 3644.44(6) | $4^-$ | 3499.53 | 144.8(1) | 0.0155(10) | | 0.038(4) |
| | | $2^+$ | 3430.12 | 214.37(12)[b] | 0.00340(12) | | |
| | | $2^+$ | 2787.30 | 857.11(8)[b] | 0.103(4) | | |
| | | $3^-$ | 2481.48 | 1163.03(8) | 1.56(5) | | 1.43(5) |
| | | $5^-$ | 2229.50 | 1414.95(15) | 0.382(12) | | 0.40(11) |
| | | $2^+$ | 1853.90 | 1790.57(12) | 1.45(4) | | 1.21(5) |
| | | $2^+$ | 1076.63 | 2567.85(15) | 2.86(10) | | 2.73(13) |
| $3^-$ | 3686.41(6) | $3^-$ | 2481.48 | 1204.87(10)[b] | 0.084(9) | | |
| | | $4^+$ | 2229.50 | 1457.02(10)[e] | 0.113(4) | | |
| | | $2^+$ | 1853.90 | 1832.27(14)[b] | 0.183(8) | | |
| | | $2^+$ | 1076.63 | 2609.76(8) | 1.69(6) | +0.040(18) | 1.50(9) |
| | | $0^+$ | 0.00 | 3686.5(3)[b] | 0.00180(10) | | |
| $(4)^{-g}$ | 3765.15(6) | $(3^-)$ | 3644.44 | 121.0(2)[b] | 0.00180(9) | | |
| | | (5) | 3555.40 | 209.68(11) | 0.0902(24) | | 0.48(2) |
| | | $4^-$ | 3499.53 | 265.59(11)[b] | 0.130(4) | | |
| | | $3, 4^{(+)}$ | 3389.62 | 375.52(10)[b] | 0.0387(12) | | |
| | | $4^+$ | 3361.39 | 403.75(10)[b] | 0.0645(19) | | |
| | | $4^-$ | 3317.54 | 447.61(8) | 0.206(8) | | 0.09(3) |
| | | $6^-$ | 3290.88 | 474.32(12) | 0.017(4) | | |
| | | $3^-$ | 3184.75 | 580.32(8) | 5.81(15) | | 5.80(17) |
| | | $5^-$ | 3055.45 | 709.69(8) | 3.54(10) | | 3.18(9) |
| | | $3^-$ | 2996.81 | 768.15(15) | 0.997(25) | | 0.39(13) |
| | | $3^+$ | 2877.90 | 887.33(8) | 0.698(21) | | 0.53(5) |
| | | $5^-$ | 2672.44 | 1092.61(8) | 1.06(3) | | 0.84(5) |
| | | $3^-$ | 2481.48 | 1283.78(10) | 0.327(10) | | 0.35(13) |
| | | $4^+$ | 2229.50 | 1535.70(10) | 0.120(4) | | 0.14(4) |
| $(4)^g$ | 3774.50(7) | $5^-$ | 3055.45 | 718.95(15) | 0.231(9) | | 0.27(4) |
| | | $5^-$ | 2672.44 | 1102.13(10) | 0.194(8) | | 0.24(3) |
| | | $3^-$ | 2481.48 | 1293.01(8)[b] | 0.396(12) | | |
| | | $4^+$ | 2229.50 | 1544.96(11)[b] | 0.0294(10) | | |
| | 3806.24(7)[a] | $4^-$ | 3317.54 | 488.64(12)[b] | 0.1084(26) | | |
| | | $5^-$ | 3055.45 | 750.70(12)[b] | 0.145(8) | | |
| | | $5^-$ | 2672.44 | 1133.72(12)[b] | 0.201(8) | | |
| | | $3^-$ | 2481.48 | 1324.75(8)[b] | 0.129(9) | | |
| | | $4^+$ | 2229.50 | 1576.75(11)[b] | 0.0230(10) | | |
| $(3^-)^g$ | 3830.57(6) | $(3^-)$ | 3644.44 | 186.2(2)[b] | 0.0360(12) | | |
| | | (5) | 3555.40 | 275.05(12)[b] | 0.0554(15) | | |
| | | $4^-$ | 3499.53 | 330.85(12) | 1.011(25) | | 1.01(3) |
| | | $4^+$ | 3361.39 | 469.04(10)[b] | 0.1120(25) | | |
| | | $3^-$ | 3184.75 | 645.87(8) | 9.80(25) | | 11.1(13) |
| | | $3^-$ | 2996.81 | 833.72(8) | 2.51(9) | | 1.8(4) |
| | | $3^+$ | 2877.90 | 952.71(8)[b] | 0.254(10) | | |
| | | $3^-$ | 2481.48 | 1349.15(8) | 3.64(9) | | 3.57(11) |
| | | $4^+$ | 2229.50 | 1601.05(8)[e] | 0.339(10) | | |

TABLE I. (*Continued.*)

| $J_i^\pi$ | $E_i$ (keV) | $J_f^\pi$ | $E_f$ (keV) | $E_\gamma$ (keV) | $I_\gamma$ | $\delta$ | $I_\gamma^{lit}$([11]) |
|---|---|---|---|---|---|---|---|
| | | $2^+$ | 1853.90 | 1976.71(8)[b] | 0.0101(5) | | |
| | | $2^+$ | 1076.63 | 2754.0(2)[b] | 0.0404(20) | | |
| $3^-$ | 3870.98(7) | $3^-$ | 3686.41 | 184.8(2)[b] | 0.00535(14) | | |
| | | | 3389.62 | 481.32(14)[b] | 0.0092(5) | | |
| | | $2^+$ | 2641.15 | 1229.88(10)[b] | 0.0272(11) | | |
| | | $4^+$ | 2229.50 | 1641.62(15)[b] | 0.0259(9) | | |
| | | $2^+$ | 1853.90 | 2016.83(11) | 0.165(6) | | 0.16(2) |
| | | $2^+$ | 1076.63 | 2794.29(12) | 0.296(9) | | 0.25(2) |
| | | $0^+$ | 0.0 | 3871.2(5)[b] | <0.0014 | | |
| | 3898.28(21) | $2^+$ | 1076.63 | 2821.6(2)[b] | 0.0247(8) | | |
| | 3904.00(7)[a] | $4^+$ | 2229.50 | 1674.55(8)[b] | 0.0244(8) | | |
| | | $2^+$ | 1853.90 | 2049.9(2)[b] | 0.0098(10) | | |
| | | $2^+$ | 1076.63 | 2827.28(8)[b] | 0.0533(15) | | |
| $(4^-)$[g] | 3925.41(6) | | 3806.24 | 118.96(12)[e] | 0.231(9) | | |
| | | (5) | 3555.40 | 369.90(8) | 0.480(15) | | 1.00(5) |
| | | $4^-$ | 3499.53 | 425.83(10) | 0.291(10) | | 0.37(2) |
| | | $4^-$ | 3317.54 | 607.87(8) | 1.62(5) | | 2.44(18) |
| | | $6^-$ | 3290.88 | 634.52(8) | 0.220(17) | | 0.11(4) |
| | | $3^-$ | 3184.75 | 740.57(9) | 1.15(3) | | 1.65(6) |
| | | $5^-$ | 3055.45 | 869.99(11)[b] | 0.448(12) | | |
| | | $3^-$ | 2996.81 | 929.0(3)[e,i] | 0.173(6) | | |
| | | $5^-$ | 2672.44 | 1253.04(8) | 1.86(8) | | 1.86(6) |
| | | $3^-$ | 2481.48 | 1444.03(9)[b] | 0.0678(20) | | −− |
| | | $4^+$ | 2229.50 | 1696.00(8) | 0.911(25) | | 0.77(2) |
| $3^-$ | 3941.98(6) | $(3, 4^+)$ | 3490.86 | 450.89(15)[b] | 0.0457(20) | | 0.09(3) |
| | | $3^-$ | 2996.81 | 945.08(9)[b] | 0.0772(18) | | |
| | | $3^+$ | 2877.90 | 1064.13(9)[e] | 0.0757(18) | | |
| | | $2^+$ | 2641.15 | 1300.82(10)[b] | 0.0434(24) | | |
| | | $4^+$ | 2229.50 | 1712.46(9)[b] | 0.0715(18) | | |
| | | $2^+$ | 1853.90 | 2088.10(8) | 0.343(11) | | 0.30(3) |
| | | $2^+$ | 1076.63 | 2865.36(8)[c] | 0.531(15) | −0.003(14) | 0.46(8) |
| $4^-$[f] | 3968.32(6) | $4^-$ | 3499.53 | 468.73(10) | 0.175(7) | | 0.36(3) |
| | | | 3389.62 | 578.7(2)[b] | 0.00594(23) | | |
| | | $4^+$ | 3361.39 | 606.90(8)[b] | 0.0394(15) | | |
| | | $3^-$ | 3184.75 | 783.48(12) | 0.320(12) | | 0.32(4) |
| | | $5^-$ | 3055.45 | 912.9(2)[b] | 0.0773(22) | | |
| | | $3^-$ | 2996.81 | 971.56(8) | 0.327(14) | −0.59(23) | 0.33(4) |
| | | $5^-$ | 2672.44 | 1296.03(12) | 0.575(15) | | 0.66(4) |
| | | $3^-$ | 2481.48 | 1486.83(8)[b] | 0.0223(8) | | |
| | | $4^+$ | 2229.50 | 1738.65(20)[b] | 0.051(3) | | |
| $(3, 4^+)$ | 4144.67(8) | $(4)^-$ | 3765.14 | [380] | [d] | | 0.55(4) |
| | | $2^+$ | 2641.15 | 1503.40(12)[b] | 0.0067(5) | | |
| | | $2^+$ | 1853.90 | 2290.78(12) | 0.0405(12) | | 0.15(1) |
| | | $2^+$ | 1076.63 | 3068.04(20) | 0.234(7) | | 0.14(2) |
| | | $0^+$ | 0.0 | 4144.7(20)[b] | <0.0001 | | |
| | 4203.40(21)[a] | $2^+$ | 1076.63 | 3126.71(20)[b] | 0.0054(3) | | |
| $(3^-, 4)$[g] | 4205.41(7) | $5^-$ | 3055.45 | [1150.34] | [d] | | *W* |
| | | $3^+$ | 2877.90 | 1327.54(8) | 0.171(9) | | 0.11(5) |
| | | $5^-$ | 2672.44 | 1532.99(8) | 0.250(7) | | 0.27(4) |
| | | $3^-$ | 2481.48 | 1723.76(11) | 0.691(16) | | 0.67(5) |
| | 4224.93(11)[a] | $4^+$ | 2229.50 | 1995.3(2)[b] | 0.0053(4) | | |
| | 4394.63(9)[a] | | 4224.94 | 169.7(2)[b] | 0.00261(11) | | |
| | | $4^-$ | 3499.53 | 895.07(12)[b] | 0.0866(22) | | |
| | | $6^-$ | 3290.88 | 1103.69(12) | 0.033(4) | | |
| | | $5^-$ | 3055.45 | 1339.25(12)[b] | 0.0802(24) | | |

TABLE I. (*Continued.*)

| $J_i^\pi$ | $E_i$ (keV) | $J_f^\pi$ | $E_f$ (keV) | $E_\gamma$ (keV) | $I_\gamma$ | $\delta$ | $I_\gamma^{lit}$([11]) |
|---|---|---|---|---|---|---|---|
| $3^-$ | 4408.81(12) | $2^+$ | 2787.30 | 1621.60(15)[b] | 0.0061(4) | | |
| | | $4^+$ | 2229.50 | 2179.2(2)[b] | 0.0295(10) | | |
| | | $2^+$ | 1076.63 | 3332.0(2) | 0.205(8) | 0.15(2) | |
| | | $0^+$ | 0.0 | 4409(2)[b] | <0.00014 | | |
| $(3^-, 4, 5^-)$ | 4441.09(8)[a] | | 4224.93 | 216.0(3)[b] | 0.00032(4) | | |
| | | (4) | 3774.50 | 666.59(8)[b] | 0.0044(3) | | |
| | | $5^-$ | 3055.45 | 1385.70(12)[b] | 0.0824(22) | | |
| | | $5^-$ | 2672.44 | 1768.62(10)[b] | 0.0949(25) | | |
| | | $3^-$ | 2481.48 | 1959.5(2)[b] | 0.0089(6) | | |
| | 4445.54(21)[a] | $2^+$ | 1076.63 | 3368.84(20)[b] | 0.0064(5) | | |
| $(3^-, 4)$[g] | 4448.97(6)[a] | | 4224.93 | 223.9(2)[b] | 0.00076(5) | | |
| | | $4^-$ | 3499.53 | 949.55(8)[b] | 0.0134(5) | | |
| | | $5^-$ | 3055.45 | 1393.6(2)[e] | 0.0209(10) | | |
| | | $3^-$ | 2996.81 | 1452.21(8)[b] | 0.0473(12) | | |
| | | $3^+$ | 2877.90 | 1570.96(11)[b] | 0.0152(6) | | |
| | | $5^-$ | 2672.44 | 1776.6(2)[b] | 0.0101(5) | | |
| | | $3^-$ | 2481.48 | 1967.41(8)[b] | 0.0492(14) | | |
| | | $4^+$ | 2229.50 | 2219.35(8)[b] | 0.0523(15) | | |
| $(3^-, 4)$[g] | 4465.82(7)[a] | | 4224.93 | 240.9(2)[e] | 0.00054(4) | | |
| | | $4^-$ | 3499.53 | 966.24(12)[b] | 0.0138(4) | | |
| | | $5^-$ | 3055.45 | 1410.3(2)[b] | 0.0879(22) | | |
| | | $3^-$ | 2996.81 | 1469.1(2)[b] | 0.0141(4) | | |
| | | $3^+$ | 2877.90 | 1587.87(8)[b] | 0.0309(12) | | |
| | | $3^-$ | 2481.48 | 1984.37(8)[b] | 0.0481(16) | | |
| $(3, 4^+)$[g] | 4497.75(7)[a] | $3^-$ | 2996.81 | 1500.92(8)[b] | 0.0528(15) | | |
| | | $3^+$ | 2877.90 | 1619.82(8)[b] | 0.0270(8) | | |
| | | $2^+$ | 2787.30 | 1710.6(3)[b] | 0.00432(15) | | |
| | | $4^+$ | 2229.50 | 2268.24(12)[b] | 0.0147(7) | | |
| | 4580.20(21)[a] | $2^+$ | 1076.63 | 3503.49(20)[b] | 0.0167(11) | | |
| | 4608.46(8)[a] | (5) | 3555.40 | 1053.2(3)[b] | 0.0122(4) | | |
| | | $5^-$ | 2672.44 | 1935.97(8)[e] | 0.00431(14) | | |
| | | $3^-$ | 2481.48 | 2126.97(8)[e] | 0.0603(22) | | |
| $(3^-, 4, 5^-)$[g] | 4691.13(8)[a] | | 4224.93 | 466.4(3)[b] | 0.00170(9) | | |
| | | $3^-$ | 3686.41 | 1004.67(12)[b] | 0.0075(3) | | |
| | | $5^-$ | 3055.45 | 1635.73(8)[b] | 0.0674(23) | | |
| | | $5^-$ | 2672.44 | 2018.48(15)[b] | 0.0262(15) | | |
| | | $3^-$ | 2481.48 | 2209.6(2)[b] | 0.0102(5) | | |
| | 4713.58(18) | $4^+$ | 2229.50 | 2484.2(3) | 0.0118(5) | 0.05(1) | |
| | | $2^+$ | 1076.63 | 3636.80(20)[b] | 0.057(2) | | |
| | 4751.27(11)[a] | | 3389.62 | 1361.63(8)[b] | 0.00351(23) | | |
| | 4848.80(22)[a] | $3^-$ | 3184.75 | 1663.9(3)[e] | 0.00284(15) | | |
| | | $4^+$ | 2229.50 | 2619.4(3)[e] | 0.0085(3) | | |
| | 4894.54(21)[a] | $4^+$ | 2229.50 | 2665.0(2)[b] | 0.00403(19) | | |
| | 4956.08(24) | $2^+$ | 2641.15 | 2314.9(4)[b] | 0.0033(3) | | |
| | | $4^+$ | 2229.50 | 2726.4(4)[b] | 0.00551(23) | | |
| | | $2^+$ | 1076.63 | 3879.5(4) | 0.0553(15) | 0.06(5) | |

[a]Newly observed level populated in the $\beta$ decay of $^{86}$Y.
[b]Newly observed $\gamma$-ray transition in the $\beta$ decay of $^{86}$Y.
[c]Placement differs from that proposed in Ref. [11].
[d]No support was found in the present work for the transition or level proposed in Ref. [11].
[e]Placement of previously tentative [10] transitions was confirmed in the present work.
[f]The $J^\pi$ assignment newly assigned based on angular correlation measurements in the present work.
[g]$J^\pi$ assignment deduced from decay pattern and log $ft$ value.
[h]Tenative $J^\pi$ assignment in Ref. [10] confirmed in angular correlation measurements in the present work.
[i]Wide, possible doublet.

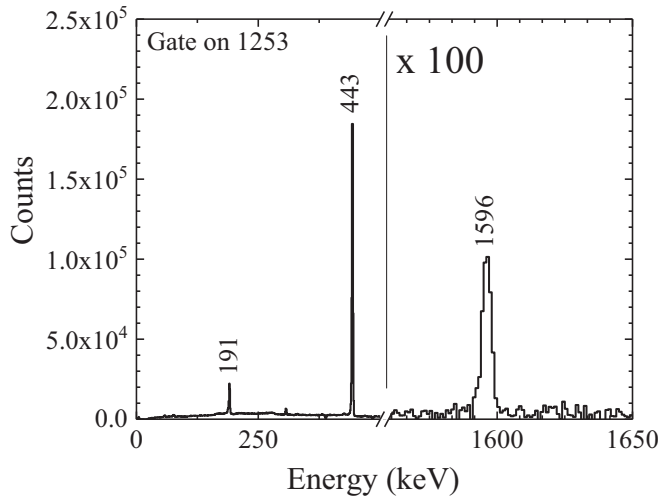


FIG. 3. Spectrum obtained by gating on the 1253-keV transition which feeds the $J^\pi = 5^-$ level at 2672 keV. Two previously identified depopulating transitions of 191 and 443 keV are observed, along with a new 1596-keV transition which corresponds to an $E3$ decay to the $2_1^+$ state. Note that the spectrum above 1550 keV has been multiplied by 100.

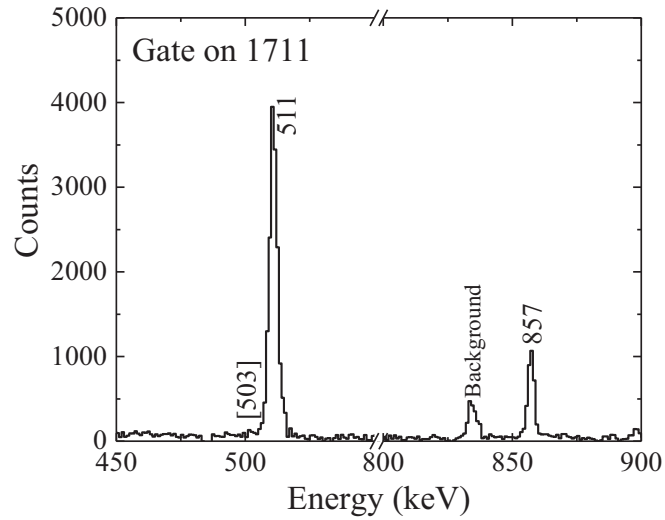


FIG. 5. Spectrum obtained through a gate on the 1711 keV, $2_4^+ \rightarrow 2_1^+$ transition which depopulates the 2787 level, illustrating the non-observation of a proposed 503-keV transition. Based on the literature intensities [11], the 503-keV transition should be similar to the clearly visible 857-keV transition.

the 1076.7-keV, $2_1^+ \rightarrow 0_1^+$ transition. Evidence for the new transition is given in Fig. 3, with a gate from above on the 1253-keV transition which feeds into the 2672-keV level; the strong 191- and 433-keV transitions are observed, along with a new, significantly weaker 1596-keV depopulating transition.

The yrast $6^+$ state at 2857 keV was not observed previously in $\beta$ decay [11]. In the present work, the 627.2-keV $6_1^+ \rightarrow 4_1^+$ transition, which is a doublet with the much stronger 627.5 keV, $3_1^- \rightarrow 2_2^+$ transition, was observed. Evidence for this transition is given in Fig. 4 using a gate on the $4_1^+ \rightarrow 2_1^+$ transition. Additionally, two new transitions of 434.21 and 698.84 keV are found to populate the 2857-keV level.

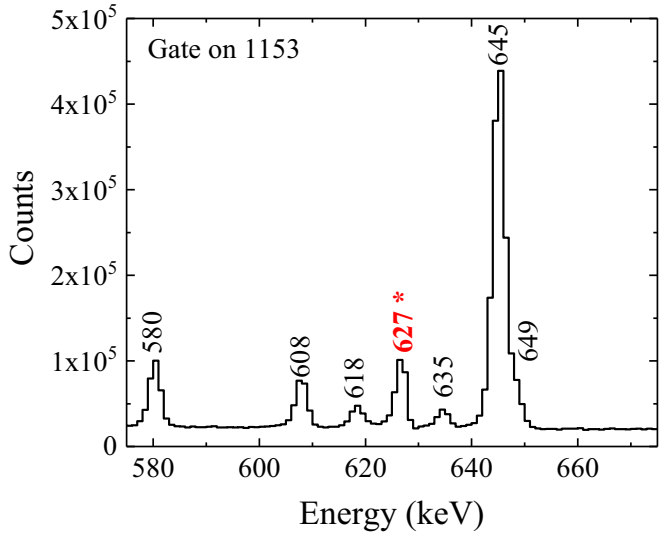


FIG. 4. Spectrum obtained by gating on the 1153-keV, $4_1^+ \rightarrow 2_1^+$ transition providing evidence for the observation of the 627 keV, $6_1^+ \rightarrow 4_1^+$ transition.

The $6^-$ level at 3291 keV was previously observed [11] to decay by three transitions of 235, 503, and 618 keV to the $5_2^-$, $2_4^+$, and $5_1^-$ levels, respectively. The current $J^\pi$ assignments would then imply a rare $M4 + E5$ character for the proposed 503-keV transition. In a gate on the 1711-keV, $2_4^+ \rightarrow 2_1^+$ transition, as shown in Fig. 5, no evidence was found for a 503-keV transition. Note that the 857-keV transition, clearly observed in Fig. 5, was also placed as populating the $2_4^+$ level with a similar intensity to the intensity previously established for the 503-keV transition [11]. Thus, the present experiment finds no evidence for the 503-keV transition. A new decay path of the 3291-keV level is established, through a 434.2-keV transition which feeds into the yrast $6^+$ level.

The high-lying states observed in the early $\beta$ decay studies tended to primarily decay to the $2^+$ 1077-keV level as well as the second $2^+$ 1854-keV level [11]. The observation of additional states at high excitation energy in $^{86}$Sr is enhanced in the present work due to the superior efficiency of Gammasphere for high energy $\gamma$ rays. While a few new levels are observed with strong decays to the first $2^+$ levels (see Table I) we identify many more new levels where the decay is highly fragmented and the depopulating $\gamma$-ray transitions primarily feed into the low-lying $3^-$, $4^+$, and $5^-$ levels. An example is given in Fig. 6, using a gate on the 826-keV, $5_2^- \rightarrow 4_1^+$ transition. The newly observed 1339-, 1386-, 1394-, and 1410-keV transitions originate from newly observed levels at 4395, 4441, 4449, and 4466 keV, respectively.

### B. Angular correlation analysis

An angular correlation analysis was also performed to determine level spins and multipole mixing ratios of transitions, with the results included in Table I. These correlations do not

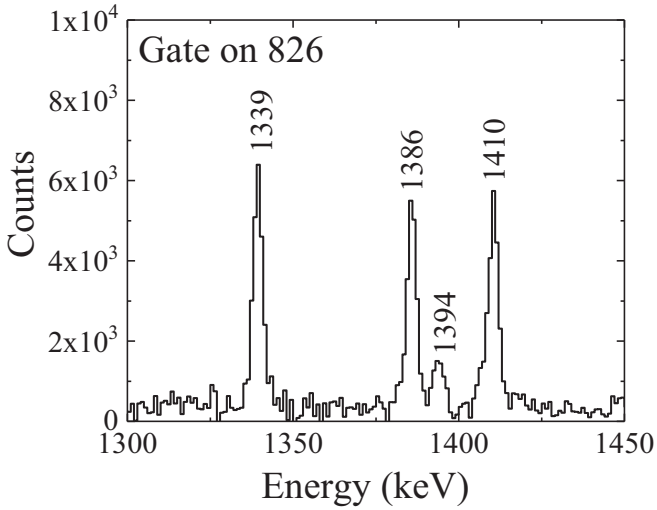


FIG. 6. A gate on the 826-keV, $5_2^- \rightarrow 4_1^+$ transition illustrating the decay of newly observed, high-excitation energy levels.

directly influence any aspects of medical imaging, however, they do contain important nuclear structure information and so are included here for completeness. The angular correlation analysis was limited to the strong transitions in the decay of $^{86}$Y and in most cases the 0°–90° and 90°–180° data were analyzed independently. An example of the angular correlation analysis is shown in Fig. 7 for the 1153-keV—1076-keV $4 \rightarrow 2 \rightarrow 0$ cascade with the data in excellent agreement with theoretical predictions. Our results are also broadly consistent with the previous angular correlation experiment [12]. For example, for the decay of the second $2^+$ state, the mixing ratio of the 777-keV transition was previously reported as $\delta = +0.251(17)$ [12], whereas our current angular correlation analysis yields $\delta = +0.33(5)$.

The 2878-keV level was previously assigned as a $J^\pi = (4)^+$ state [10], based on L($^3$He, $d$) = 1 from a $5/2^-$ target

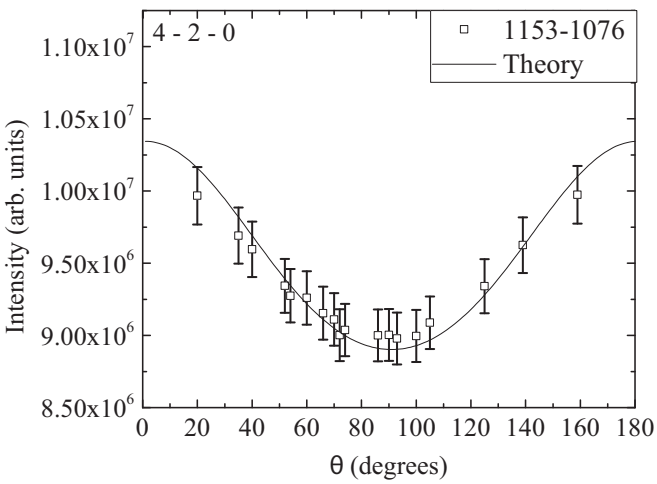


FIG. 7. Angular correlation analysis for the 1153-1076 keV cascade. Data are given as open symbols compared to the theoretical prediction for a $4 \rightarrow 2 \rightarrow 0$ cascade.

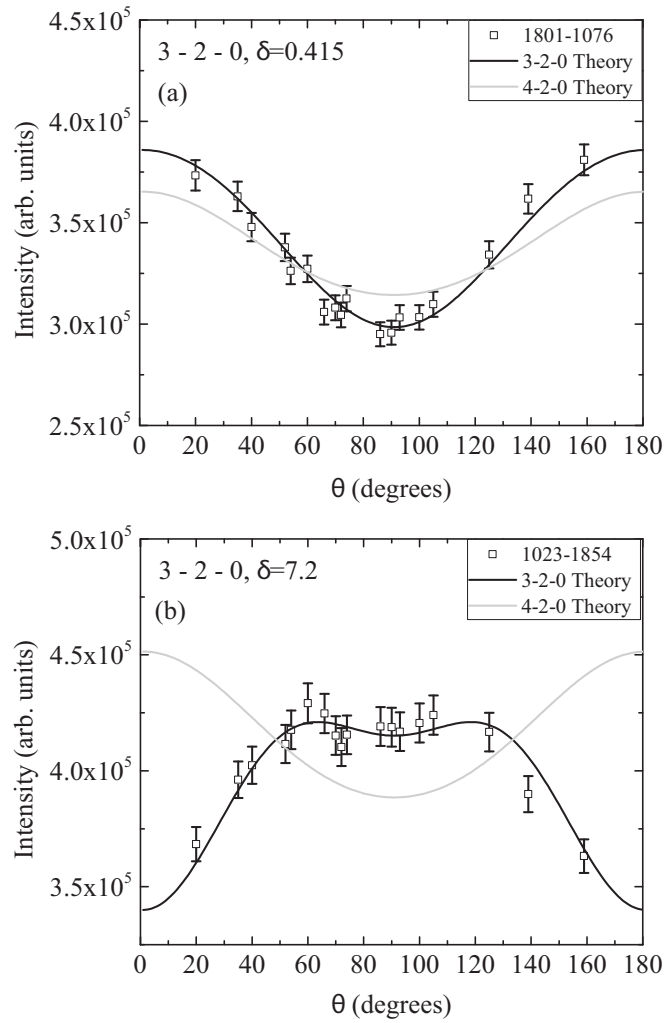


FIG. 8. Angular correlation analysis for the (a) 1801-1076 and (b) 1023-1854 cascades. The data (open symbols) are compared to theoretical predictions (solid lines) in (a) for a 4-2-0 cascade and a 3-2-0 cascade with a mixing ratio of 0.415 and in (b) for a 4-2-0 cascade and a 3-2-0 cascade with a mixing ratio of +7.2.

and decay and population patterns. In the present work, the analysis for both the 1023-1853 keV and 1801-1076 keV cascades strongly favors a $J = 3$ assignment for the 2878-keV level. These two angular correlation results are given in Fig. 8 and are compared with $4 \rightarrow 2 \rightarrow 0$ and $3 \rightarrow 2 \rightarrow 0$ theoretical cascades. Only the latter theoretical prediction is found to be consistent with the current $\gamma\gamma(\theta)$ data. Our result is still consistent with the $L$ transfer and decay and population patterns, which allowed for possible $J^\pi$ values of $(3, 4)^+$. Combining our angular correlation measurement with the transfer measurement we can rigorously assign $J^\pi = 3^+$ for the 2878-keV level. Furthermore, the 1023-keV transition was found to be a mixture of $M1 + E2$ with $\delta = +0.43(3)$ while the 1801-keV transition was found to be predominantly $E2$ in character [$\delta = +7.2(13)$]. Our result is consistent with a recent $(p, 2n)$ in-beam study [24] of $^{86}$Sr which also determined $J = 3$ for the 2878-keV level.

Similarly, the 3317-keV level was previous assigned [26,27] as $J^\pi = (5)^-$ based on $L(d,t) = 1$ using a target with $J^\pi = 9/2^+$ and $L(p,t) = 5$ in Ref. [25]. The previous $J^\pi$ assignment before Ref. [25] for this level was given as $(3,4,5)^-$. Careful inspection of the $(p,t)$ data shown in Ref. [25] shows that the cross section is rather featureless as a function of $\theta$ and cast some doubt on the reliability of $L(p,t) = 5$. Using the 835-627 cascade in the present work, it was found that the 3317-keV level is well described with only $J = 4$. The angular correlation used does not agree with a 5-3-2 theory cascade for all possible delta. Therefore, using the $L(d,t) = 1$ determination and the $J = 4$ found in the present work, the 3317-keV level is assigned to $J^\pi = 4^-$.

For several levels, the data evaluation [10] restricted the spin and parity to a range of values. By combining our angular correlation analysis with prior measurements, a unique spin and parity assignment could often be made. An example of this is the 3499-keV level which was previously assigned [26,27] to be $(3,4,5)^-$, by a $L(d,t) = 1$ and $L(p,d) = 3$ using a target with $J^\pi = 9/2^+$. Using the 1270-1153 cascade, the spin was determined to be a 4. By combining these experimental data, we assign $J^\pi = 4^-$ to the 3499-keV level. In addition, the $\delta$ value for the 1270-keV transition, $\delta = -0.05(9)$, obtained in this work is consistent with a pure $E1$ transition.

## V. DISCUSSION

The data collected in this high statistics experiment has allowed observation of $\gamma$-ray transitions with intensities down to a level of $10^{-6}$ that of the strongest, 1076-keV, $2_1^+ \rightarrow 0_1^+$ transition. This gives confidence that we can reliably deduce the $\beta$ feedings to individual levels using a $\gamma$-ray intensity balance. $^{86}$Y has a ground state spin/parity of $J^\pi = 4^-$ [10]. Thus, the ground state to ground state decay is $\Delta J = 4$, $\Delta\pi =$ yes, requiring a log $ft$ of at least 21 [28] implying that the total $I_{\beta+\epsilon}$ to the ground state of $^{86}$Sr be $<1 \times 10^{-10}$. Therefore, to convert the measured relative intensities to an absolute scale, the decay scheme can be normalized by determining the total flux of transitions directly populating the ground state. Using the sum of all $\gamma$ rays and conversion electrons (ce) directly populating the ground state, we infer that the 1076-keV, $2_1^+ \rightarrow 0_1^+$ $\gamma$ ray is present in 82.66(17)% of the decays. This compares very well with the previous evaluated absolute intensity of 82.5(4)% [10,11]. This small change is perhaps not surprising, as due to the high-spin of the parent, it is unlikely to observe a number of new transitions which decay directly to the ground state.

Using the absolute $\gamma$-ray intensities, the total $\beta^+ + \epsilon$ feeding for each energy level can be calculated from a $\gamma$-ray intensity balance at each level. This is explicitly calculated as $\Sigma I^{\rm out}_{\gamma+{\rm ce}} - \Sigma I^{\rm in}_{\gamma+{\rm ce}} = I(\beta^+ + \epsilon)$. The total $I(\beta^+ + \epsilon)$ feedings to each level deduced from the present measurement are given in Table II. Of the many new levels given in Table I, most of the new transitions observed in this work come from levels at very high excitation energy in $^{86}$Sr and rain down to populate the low-lying states. Thus, we find that while the strong $\gamma$ transitions from the lowest states have intensities which are consistent with previous works, the distribution of

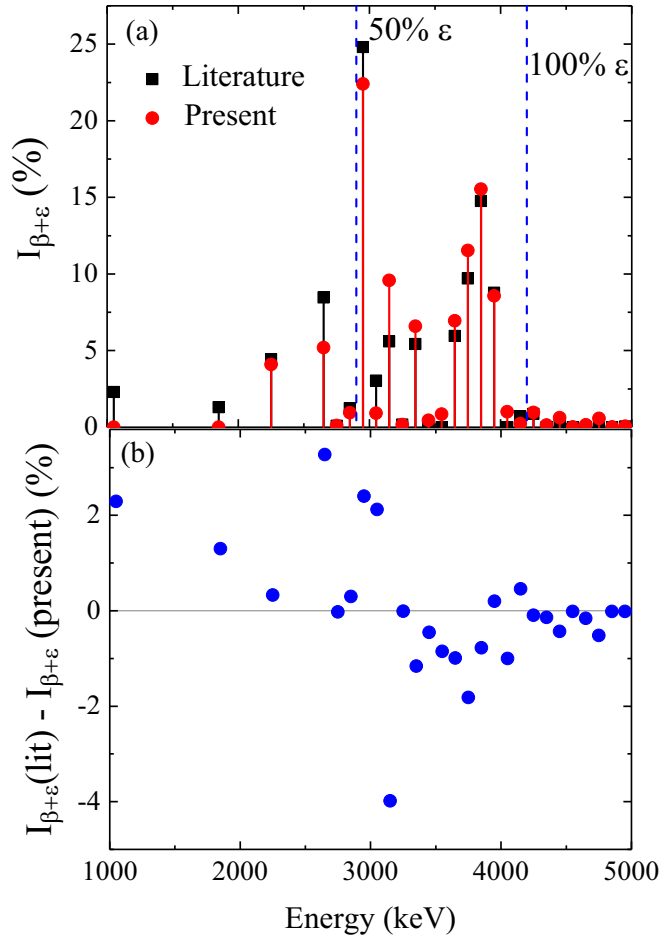


FIG. 9. Comparison between the literature $\beta$ feeding [10] and those obtained in the present work. (a) Total $I_{\beta+\epsilon}$ feedings derived from the present work (red circles) compared with the literature feedings (black squares). Dashed vertical lines represent the energies where the feeding shifts from $\beta^+$ to primarily electron capture ($\epsilon$). (b) Difference between the total literature feedings and those derived from the present work.

population from the $\beta^+ + \epsilon$ decay has been shifted to much higher excitation energy. The change in the $\beta^+ + \epsilon$ feeding, compared to the literature, is shown in Fig. 9. The weak decay process has two mechanisms; positron emission and electron capture. For decays with $Q$ values less than 1022 keV, only electron capture occurs, whereas positron emission rapidly takes over for higher decay energies, due to its three body phase space. At lower energies, where $\beta^+$ decay dominates, all feedings are reduced compared to the literature [10]. For higher energies, where electron capture decay becomes more prominent, the feedings to those levels then increases. The net result from the current work is to shift the $\beta$ feeding pattern to higher excitation energy and thus enhance the electron capture contribution and reduce the positron emission.

The ratio of electron capture decay to positron decay is calculated using the formalization of Gove and Martin [29] and a total decay $Q$ value of 5240(14) keV [30]. Applying these ratios to our deduced total $\beta^+ + \epsilon$ feeding allows us to determine the individual $\beta^+$ and $\epsilon$ feeding to each level, which

TABLE II. $\beta$ feeding intensities derived from the $\gamma$-ray measurements following the decay of $^{86}$Y. Total feeding intensities are derived from an intensity imbalance at each level, while the individual $I\beta^+$ and $I\epsilon$ components are calculated using formalism in Ref. [29]. log $ft$ values are calculated from the feeding intensities using a $Q$ value of 5240(14) [30] and a half-life of 14.74(2) h [10]. Also included are the maximum ($E_{max}$) and average ($E_{mean}$) positron energies for each decay. See text for description on the positron energy calculation.

| $J^\pi$ | $E_{level}$ (keV) | $I\beta^+$ % | $I\epsilon$ % | $I$(tot) % | log $ft$ | $E^{e^+}_{max}$ (keV) | $E^{e^+}_{mean}$ (keV) |
|---|---|---|---|---|---|---|---|
| $2^+$ | 1076.6 | <0.5 | <0.08 | <0.6 | >10.9[1u] | 3141(14) | 1437(7) |
| $2^+$ | 1853.9 | <0.4 | <0.2 | <0.6 | >10.2[1u] | 2364(14) | 1078(7) |
| $4^+$ | 2229.5 | 3.7(7) | 0.87(17) | 4.6(9) | 7.7(1) | 1989(14) | 883(7) |
| $3^-$ | 2481.5 | 2.8(7) | 0.99(24) | 3.8(9) | 7.6(1) | 1737(14) | 768(6) |
| $2^+$ | 2641.2 | <0.004 | <0.006 | <0.01 | >11.2[1u] | 1577(14) | 721(6) |
| $5^-$ | 2672.4 | 3.4(4) | 1.8(2) | 5.2(6) | 7.27(4) | 1546(14) | 681(6) |
| $2^+$ | 2787.3 | 0.035(3) | 0.079(6) | 0.114(9) | 9.9(1)[1u] | 1431(14) | 655(6) |
| $6^+$ | 2856.6 | 0.01(1) | 0.04(4) | 0.05(5) | 10.3(5)[1u] | 1361(14) | 624(6) |
| $3^+$ | 2877.9 | 0.4(2) | 0.4(1) | 0.8(3) | 7.9(2) | 1340(14) | 589(6) |
| $3^-$ | 2996.8 | 10.5(4) | 11.4(4) | 21.9(7) | 6.34(2) | 1221(14) | 535(6) |
| $5^-$ | 3055.5 | 0.40(7) | 0.52(9) | 0.92(16) | 7.66(8) | 1163(14) | 510(6) |
| $(3, 4^+)$ | 3133.5 | 0.0433(19) | 0.070(3) | 0.113(4) | 8.50(2) | 1085(14) | 475(6) |
| $(3, 4^+)$ | 3175.5 | 0.024(1) | 0.045(2) | 0.069(3) | 8.68(3) | 1043(14) | 456(6) |
| $3^-$ | 3184.8 | 3.3(2) | 6.1(4) | 9.4(6) | 6.53(3) | 1033(14) | 452(6) |
| $6^-$ | 3290.9 | 0.02(1) | 0.04(4) | 0.06(5) | 9.1(2)[2n] | 927(14) | 430(6) |
| $4^-$ | 3317.5 | 1.54(8) | 4.62(15) | 6.16(18) | 6.60(2) | 900(14) | 394(6) |
| $4^+$ | 3361.4 | 0.098(5) | 0.349(12) | 0.447(14) | 7.70(2) | 857(14) | 375(6) |
| | 3389.6 | 0.0028(4) | 0.0110(14) | 0.0138(18) | 9.19(6) | 828(14) | 363(6) |
| $2^+$ | 3430.1 | 0.00179(14) | 0.0402(13) | 0.0420(13) | 9.70(2)[1u] | 788(14) | 370(6) |
| $(3, 4^+)$ | 3490.9 | 0.013(1) | 0.079(4) | 0.092(4) | 8.28(3) | 727(14) | 318(6) |
| $4^-$ | 3499.5 | 0.042(6) | 0.28(3) | 0.32(4) | 7.73(6) | 718(14) | 314(6) |
| (5) | 3555.4 | 0.134(10) | 1.17(4) | 1.30(4) | 7.08(2) | 663(14) | 291(6) |
| $(3^-)$ | 3644.4 | 0.34(3) | 4.90(10) | 5.24(10) | 6.41(2) | 574(14) | 252(6) |
| $3^-$ | 3686.4 | 0.084(9) | 1.62(6) | 1.70(6) | 6.87(2) | 532(14) | 234(6) |
| $(4)^-$ | 3765.2 | 0.30(4) | 10.54(17) | 10.84(17) | 6.01(2) | 453(14) | 201(6) |
| (4) | 3774.5 | 0.0182(22) | 0.682(15) | 0.700(15) | 7.19(2) | 444(14) | 197(6) |
| | 3806.2 | 0.0061(9) | 0.304(16) | 0.310(16) | 7.53(3) | 412(14) | 183(6) |
| $(3^-)$ | 3830.6 | 0.23(3) | 14.6(3) | 14.8(3) | 5.83(2) | 387(14) | 173(6) |
| $3^-$ | 3871.0 | 0.0045(7) | 0.433(10) | 0.438(10) | 7.33(2) | 347(14) | 156(6) |
| | 3898.3 | 0.00015(3) | 0.0202(8) | 0.0204(8) | 8.64(2) | 320(14) | 144(6) |
| | 3904.0 | 0.00051(9) | 0.0718(18) | 0.0723(18) | 8.09(2) | 314(14) | 142(6) |
| $(4^-)$ | 3925.4 | 0.031(6) | 5.78(10) | 5.81(10) | 6.17(2) | 293(14) | 133(6) |
| $3^-$ | 3942.0 | 0.0041(9) | 0.978(16) | 0.982(16) | 6.93(2) | 276(14) | 126(6) |
| $4^-$ | 3968.3 | 0.0037(9) | 1.32(3) | 1.32(3) | 6.78(2) | 250(14) | 114(6) |
| $(3,4^+)$ | 4144.7 | | 0.232(7) | 0.232(7) | 7.41(2) | | |
| | 4203.4 | | 0.0045(3) | 0.0045(3) | 9.07(4) | | |
| $(3^-,4)$ | 4205.4 | | 0.919(17) | 0.919(17) | 6.76(2) | | |
| | 4224.9 | | <0.0003 | <0.0003 | >10.2 | | |
| | 4394.6 | | 0.167(6) | 0.167(6) | 7.32(3) | | |
| $3^-$ | 4408.8 | | 0.199(8) | 0.199(8) | 7.23(2) | | |
| $(3^-, 4, 5^-)$ | 4441.1 | | 0.158(4) | 0.158(4) | 7.30(2) | | |
| | 4445.5 | | 0.0053(5) | 0.0053(5) | 8.76(5) | | |
| $(3^-,4)$ | 4449.0 | | 0.173(3) | 0.173(3) | 7.25(2) | | |
| $(3^-,4)$ | 4465.8 | | 0.161(4) | 0.161(4) | 7.26(2) | | |
| $(3,4^+)$ | 4497.8 | | 0.0817(16) | 0.0817(16) | 7.52(2) | | |
| | 4580.2 | | 0.0138(10) | 0.0138(10) | 8.18(4) | | |
| | 4608.5 | | 0.0635(20) | 0.0635(20) | 7.48(3) | | |
| $(3^-, 4, 5^-)$ | 4691.1 | | 0.094(3) | 0.094(3) | 7.19(3) | | |
| | 4713.6 | | 0.0569(17) | 0.0569(17) | 7.37(3) | | |
| | 4751.3 | | 0.00290(20) | 0.00290(20) | 8.59(4) | | |
| | 4848.8 | | 0.0094(4) | 0.0094(4) | 7.88(4) | | |
| | 4894.5 | | 0.00333(17) | 0.00333(17) | 8.22(5) | | |
| | 4956.1 | | 0.0530(13) | 0.0530(13) | 6.84(5) | | |

are included in Table II. This calculation has a dependence on the spins of the initial and final levels, which defines whether the transitions are allowed or forbidden. For levels where $\beta^+$ decay is energetically allowed, most of the $J^\pi$ values are well established, thus defining the character of the transitions. In the calculation, first forbidden nonunique transitions are assumed to have the same shape as allowed transitions, which is a common approximation [31]. In the energetically allowed $\beta^+$ window there are four levels with no $J^\pi$ assignment. These levels are high in excitation energy with weak feeding, $I\beta^+ < 0.01\%$, and we find that varying the degree of forbiddenness does not change significantly the results discussed below. For three first-forbidden unique transitions to the 1076.6-, 1853.9-, and 2641.2-keV levels, the feeding is consistent with zero within the uncertainties. For subsequent calculations the upper limits are symmetrized, i.e., <0.4% is taken as 0.2(2)%.

With the shift in feeding to higher excitation energy, the deduced $\beta^+$ feeding is reduced and consequently, the number of 511 keV photons emitted per decay is reduced. With the new decay scheme, the probability that the decay involves positron creation is reduced to 27.9(12)% down from the current evaluated value of 32.5(20)% [10], a reduction of 14%. The value of 32.5(20)% currently in evaluated database [10] is derived from a $\gamma$-ray intensity balance in a similar procedure as presented here, using data from Ref. [11]. The positron intensity has also been directly measured. Using a double focusing beta spectrometer, Ref. [32] obtained a positron intensity of 28.4%, excluding what they believed was a possible contribution from $^{87m}$Y decay. Reference [33] used a long lens beta spectrometer and obtained a positron intensity of 31.4%. While the current value is in good agreement with the Yamazaki *et al.,* value [32], neither of these early measurements provided any uncertainty on their measured values.

The overall dose to the patient can be determined by computing the weighted mean of the photon dose and the electron dose. The dose is determined summing the product of the intensity and energy of the emitted radiation, for example, for the photon dose this is given as $\Sigma_i(E_{\gamma i} \times I_{\gamma i}) + (E_{(x-ray)i} \times I_{(xray)i})$. From the evaluated data in Ref. [10] the photon dose was 3.56(3) MeV. In the present work, the photon dose increases to 3.62(3) MeV, the majority stemming from $\gamma$ rays, with a 6.4(2) keV contribution from x rays.

The electron dose calculation is more complicated due to the continuous nature of the positron spectrum. The nuclear level to nuclear level positron spectrum following $\beta$-plus decay is given by [31]

$$S(E) = NW(W^2-1)^{1/2}(W-W_0)^2 \times F(Z_k, W) \times C(Z, W), \quad (1)$$

where $N$ is a normalization factor so $\int S(E)dE = 1$; $W$ is the relativistic kinetic energy, $W = E/m_ec^2 + 1$, and $W_0 = Q/m_ec^2 + 1$, with $Q$ the total decay energy available also known as the end-point energy; $F(Z, W)$ is the Fermi function and $Z$ is the number of protons in the daughter nucleus; $C(Z, W)$ is a correction factor that takes into account angular momentum and parity changes in the transition as well as screening, radiative and finite-size effects. The average positron energy for a given transition is calculated as

$$\langle E_k \rangle = \int S_k(E) E dE, \quad (2)$$

This energy is calculated using the LOGFT code, which can be accessed through a web application [34], and included in Table II. The average neutrino energy is then determined by $Q - \langle E_k \rangle$. The total electron dose includes contributions from the positrons, conversion electrons and Auger electrons. As the atomic number of Sr is relatively low, $Z = 38$, and the decay is composed of mainly high-energy $\gamma$ rays, the conversion electron and Auger electron dose is small, 2.2(1) keV for the former and 3.7(1) keV for the latter. The positron dose determined from the present work is 169(10) keV, an approximately 25% reduction compared to a positron dose of 212(22) keV calculated from literature data [10].

## VI. CONCLUSIONS

$^{86}$Y is a potential imaging partner to the therapeutic $^{90}$Y isotope. To ensure precise and reliable decay data are available for use in medical imaging, the decay of $^{86}$Y was studied with the Gammasphere array. The main finding is a reduction in the probability of positron emission by ∼14%, due to about 100 new $\gamma$-ray transitions being added to the decay scheme which shifts the decay strength function to higher excitation energy in the daughter. The observation of numerous additional $\gamma$ rays increases the photon dose to 3.62(3) MeV and decreases the positron dose to 169(10) keV. Finally, we were able to confirm the absolute intensity of the 1076 keV, $2_1^+ \rightarrow 0_1^+$ $\gamma$ ray as 82.66(17)%, which gives confidence for use in isotope production methods and source strength determinations.

## ACKNOWLEDGMENTS

The DOE Isotope Program is acknowledged for funding ST5001030. Work supported by the U.S. DOE under Grant No. DE-FG02-94ER40848 and Contracts No. DE-AC02-98CH10946 and No. DE-AC02-06CH11357 and by the DOE Office of Science, Office of Workforce Development for Teachers and Scientists (WDTS) under the Science Undergraduate Laboratory Internships Program (SULI). This research used resources of Argonne National Laboratory's ATLAS facility which is a DOE office of Science User Facility.

[1] S. K. Basu and E. A. McCutchan, Nucl. Data Sheets **165**, 1 (2020).
[2] Chadwick L. Wright, Jun Zhang, Michael F. Tweedle, Michael V. Knopp, and Nathan C. Hall, Biomed. Res. Int. **2015**, 481279 (2015).
[3] R. G. Selwyn, R. J. Nickles, B. R. Thomadsen, L. A. DeWerd, and J. A. Micka, Appl. Radiat. Isot. **65**, 318 (2007).
[4] H. G. Buchholz *et al.*, Eur. J. Nucl. Med. Mol. Imag. **30**, 716 (2003).
[5] P. E. N. Braad *et al.*, Phys. Med. Biol. **60**, 3479 (2015).

[6] Y. Zhou *et al.*, Adv. Drug Del. Rev. **65**, 1098 (2013).
[7] T. K. Nayak and M. W. Brechbiel, Med. Chem. **7**, 380 (2011).
[8] R. Hernandez *et al.*, Commun. Biol. **2**, 79 (2019).
[9] R. Arlt, N. G. Zaitseva, B. Kratsik, M. G. Loshchilov, G. Muziol, and C. T. Min, Bull. Acad. Sci. USSR, Phys. Ser **33**, 1463 (1970).
[10] A. Negret and B. Singh, Nucl. Data Sheets **124**, 1 (2015).
[11] A. V. Ramayya *et al.*, Phys. Rev. C **2**, 2248 (1970).
[12] A. Akbarov, B. Ibragimov, I. K. Kuldzhanov, A. I. Muminov, and R. Razhabbaev, Bull. Acad. Sci. USSR, Phys. Ser. **48**, 105 (1984).
[13] H. F. Valdovinos, R. Hernandez, T. E. Barnhart *et al.*, Appl. Radiat. Isot. **95**, 23 (2015).
[14] M. A. Avila-Rodriguez, J. A. Nye, and R. J. Nickles, Appl. Radiat. Isot. **66**, 9 (2008).
[15] F. Rosch, S. M. Qaim, and G. Stocklin, Appl. Radiat. Isot. **44**, 677 (1993).
[16] http://www.phy.anl.gov/gammasphere/doc/index.html, 7th July 2015.
[17] D. C. Radford, Nucl. Instrum. Methods Phys. Res. A **361**, 297 (1995).
[18] B. Singh and J. C. Roediger, Nucl. Data Sheets **111**, 2081 (2010).
[19] M. J. Martin, Nucl. Data Sheets **114**, 1497 (2013).
[20] E. A. McCutchan and A. A. Sonzogni, Nucl. Data Sheets **115**, 135 (2014).
[21] H. Junde, H. Su, and Y. Dong, Nucl. Data Sheets **112**, 1513 (2011).
[22] W. D. Kulp *et al.*, Phys. Rev. C **76**, 034319 (2007).
[23] T. D. Johnson and W. D. Kulp, Nucl. Data Sheets **129**, 1 (2015).
[24] H. Duckwitz, P. Petkov, T. Thomas, T. Ahn, A. Blazhev, N. Cooper, C. Fransen, M. Hinton, G. Ilie, J. Jolie, and V. Werner, Nucl. Phys. A **965**, 13 (2017).
[25] I. C. Oelrich *et al.*, Phys. Rev. C. **14**, 563 (1976).
[26] P. C. Li, W. W. Daehnick, and R. D. Rosa, Nucl. Phys. A **442**, 253 (1985).
[27] M. C. Radhakrishna, N. G. Puttaswamy, H. Nann, D. W. Miller, P. P. Singh, W. W. Jacobs, W. P. Jones, and E. J. Stephenson, Phys. Rev. C **40**, 1603 (1989).
[28] B. Singh, J. L. Rodriguez, S. S. M. Wong, and J. K. Tuli, Nucl. Data Sheets **84**, 487 (1998).
[29] N. B. Gove and M. J. Martin, At. Data Nucl. Data Tables **10**, 205 (1971).
[30] M. Wang, G. Audi, F. G. Kondev, W. J. Huang, S. Naimi, and X. Xu, Chin. Phys. C **41**, 030003 (2017).
[31] X. Mougeot, Phys. Rev. C **91**, 055504 (2015).
[32] T. Yamazaki, H. Ikegami, and M. Sakai, Nucl. Phys. A **30**, 68 (1962).
[33] B. Van Nooijen, W. Lourens, H. Van Krugten, and A. H. Wapstra, Nucl. Phys. A **63**, 241 (1965).
[34] www.nndc.bnl.gov/logft.